Int. J. Heat Mass Transfer. Vol. 15, pp. 953–968. Pergamon Press 1972. Printed in Great Britain

AXIAL HEAT TRANSFER IN PACKED BEDS. GAS FLOW THROUGH BEDS BETWEEN 20 AND 650°C

G. S. G. BEVERIDGE*

Department of Chemical Engineering, Heriot-Watt University, Edinburgh EH1 1HX, Scotland

and

D. P. HAUGHEY

Meat Industry Research Institute of New Zealand (Inc.), P.O. Box 617, Hamilton, New Zealand

(*Received* 27 *October* 1970 *and in revised form* 19 *July* 1971)

Abstract—The experimental measurements and theoretical models described in part I are extended to the case of gas flow through the bed. Temperature profile measurements are given for cocurrent gas and axial heat flows through the bed over a temperature range 20–650°C and a particle Reynolds number up to 5.

These results are analysed in terms of both a continuous (diffusion) model and a new discrete (mixing cell) model. The latter provides more quantitative information on the heat transfer mechanisms involved since, unlike the former, separate account is taken of solid conduction–radiation, solid contact resistance, as well as solid–gas convection and bulk gas flow convection. The suitability of the discrete model is verified by comparison with both the present experimental cocurrent results at low and high temperatures and with previously published countercurrent low temperature measurements using a range of packing materials.

NOMENCLATURE

a, inlet to mixing cell;
b, location of point contact in mixing cell;
B, function (Appendix 2);
c, exit from mixing cell;
C, $\sqrt{(H_D/K_D)}$;
C_g, gas specific heat;
C_i constants ($i = 1$–6, Appendices 1 and 2);
D, function (Appendix 2);
D_p, particle diameter;
E, eddy diffusivity;
F_i, defined by equations (7) and (8);
G, gas mass flow rate per unit area;
h, heat transfer coefficient;
H, convection parameter (Appendix 3b);
k, thermal conductivity of single phase system;
k_e, effective thermal conductivity of two-phase system, based on bed area;
k_{e_s}, effective thermal conductivity of solid path, based on solid area $(1 - \varepsilon)$;
K, conduction parameter (Appendices 3c and d);
J_h, dimensionless J factor for heat transfer;
l, cell length;
L, bed length;
m, number of mixing cells (Appendix 3a);
Nu, Nusselt dimensionless group;
P_D, contact resistance parameter (Appendix 3d);
Pe, Péclét dimensionless group;
Pr, Prandtl dimensionless group;
Q, heat flow in axial direction;
Q_D, Q'_D, dimensionless heat flow (Appendices 2 and 3e);
Re, Reynolds dimensionless group, based on packing size, D_p

* Present address: Department of Chemical Engineering, University of Strathclyde, Glasgow, Scotland.

S, particle surface per unit bed volume;
t, gas temperature;
$\bar{t}$, gas dimensionless temperature, $(t - T_m)/(T_0 - T_m)$;
T, solid temperature;
$\bar{T}$, solid dimensionless temperature, $(T - T_m)/(T_0 - T_m)$;
W_j, function ($j = 1$–4, Appendix 2);
X, thermal conductivity ratio (k_s/k_g);
Y, effective thermal conductivity ratio (k_e/k_g or k_{e_s}/k_g);
z, axial distance through bed or cell;
Z, Z', dimensionless axial distance through the bed and cell, $Z = z/L$, $Z' = z/l$, respectively;
ε, bulk mean void;
ρ, gas density;
ψ, tortuosity factor;
ϕ_A, ϕ_B, relative heat flow parameters (Appendix 3f).

Subscripts

a, inlet to mixing cell;
b, location of point contact in mixing cell;
c, exit from mixing cell;
g, gas phase;
o, bed inlet;
m, bed exit;
p, particle;
r, cell number in discrete model, cell inlet condition for temperatures;
s, solid phase;
C, continuous (diffusion) model;
D, discrete (mixing cell) model;
*, gas approach conditions (continuous model);
stag, stagnant bed ($Re = 0$);
1, bed exit (continuous model).

These quantities may be expressed in any set of consistent units.

1. INTRODUCTION

PART I of this paper [1] discussed the heat transfer characteristics of randomly packed beds of spherical particles for the particular case of a quiescent gas. The contribution of conduction, radiation and convection to heat transfer within the two-phase packed bed system was analysed on the basis of four conduction and three radiation mechanisms.

The analysis is now extended to include the case in which the gas flows through the void structure of the bed for conditions in the range of particle Reynolds number, Re, from 0 to 5 and temperatures of 20–650°C, the theoretical models being extended to include the additional convection mechanisms:

9. forced convection, solid–gas heat transfer
10. forced convection due to bulk flow, turbulent diffusion or mixing of the gas

the eighth mechanism, that of natural convection, being insignificant except at the lower flows.

2. EXPERIMENTAL [2]

This has been briefly described in Part I. A fan passed air through the bed to atmosphere at a controlled flow rate as measured on a variable area meter. The gas outlet temperature was measured by a specially constructed suction thermocouple incorporating radiation shields and fitted over the top of the test bed. Inlet gas temperatures were measured using a sheathed thermocouple placed at the bed inlet. Uniform velocity profiles within the bed were attained by using vanes, screens and packing in the air inlet pipes. Radial profiles obtained with a hot wire anemometer confirmed the uniformity of the mean profiles, the local variation over a particle length being due to the jet effect of the gas leaving the voids between individual particles.

All temperatures within the bed were measured within the solid particles, and, as with the stagnant gas runs, the local wall heaters were adjusted until steady state conditions were obtained for one-dimensional heat flow in the axial direction cocurrent with the gas flow.

The steady state solid temperature profiles for various gas flow rates and bed inlet temperatures are shown in Fig. 1. Figure 2 shows in

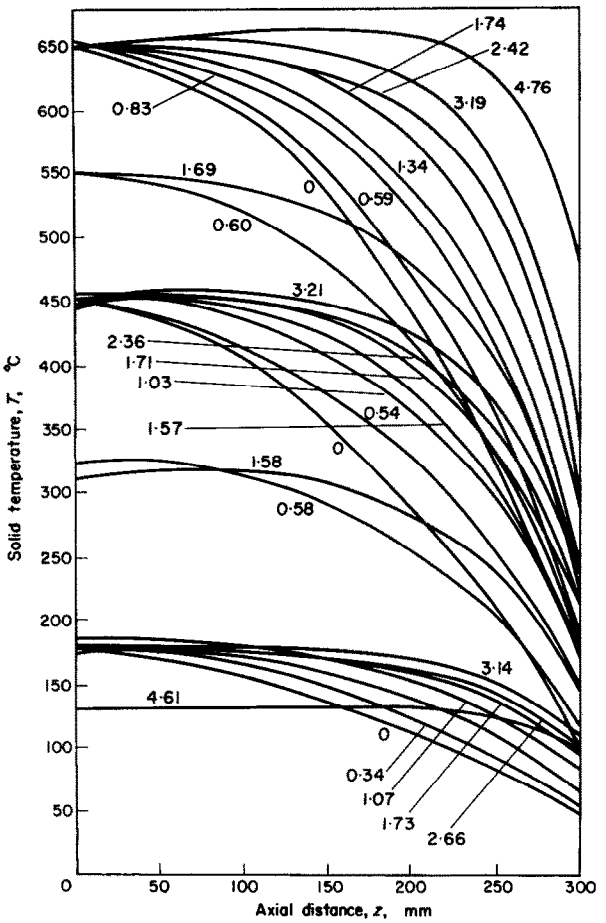

FIG. 1. Solid temperature profiles for gas flow runs (parameter refers to the particle Reynolds number values).

dimensionless form the typical effect of gas flow rate for low values of bed mean temperatures. Dimensionless profiles for lower temperatures show less curvature, but in all cases greater curvature results from a higher gas flow (forced convection) and for a higher inlet bed temperature (radiation effects and natural convection [2, 3] through the bed). Under some conditions temperature profile maxima occurred for the higher levels of gas flow rate or Reynolds number.

3. THEORY

Any evaluation of packed bed systems depends upon an ability to determine the temperature and fluid velocity patterns produced within the bed. Three classifications of model have been suggested [4], based upon the scale of the phenomena involved in terms of the variations in pattern occurring over a distance relative to the particle diameter, D_p: (a) large scale $\gg D_p$, (b) intermediate scale, $\approx D_p$, (c) small scale, $\ll D_p$. In terms of increasing complexity the types of model available may be classified as

(a) continuous deterministic models—in which the processes in one or two pseudo-homogeneous phases are formulated in terms of differential equations (e.g. [5])

(b) discrete deterministic models—in which

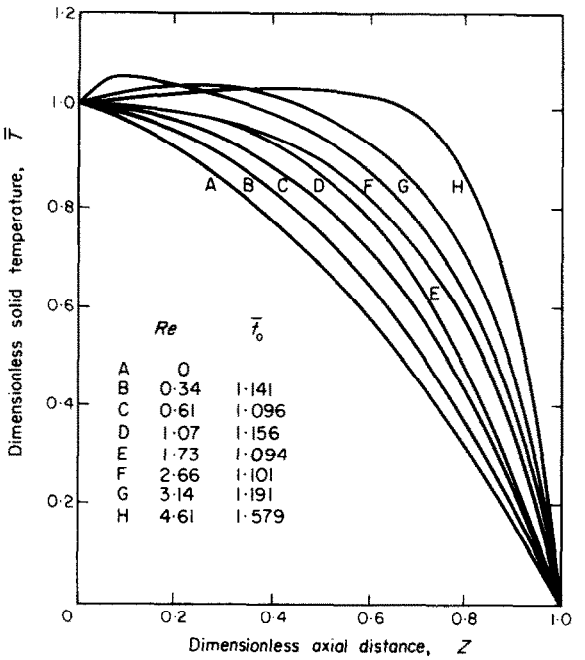

FIG. 2. Gas flow runs–effect of gas flow rate (temperature level at bed mid-point 147–175°C).

finite stage models are formulated in terms of difference equations (e.g. [5])

(c) stochastic models—in which random perturbations are allowed to occur in models of types (a) and (b) (e.g. [4, 6]).

The present analysis will be confined to the two types of deterministic model.

The continuous deterministic conduction–convection model

The validity of this model, summarised in Appendix 1 and detailed elsewhere [2], depends upon the degree of heterogeneity of the bed being much smaller than the bed size, i.e. $D_p \ll L$.

When the solid and gas temperatures are taken as being equal, the single phase general solution for a finite bed, given in Fig. 3, shows that decreasing values of the effective thermal conductivity, K_C, increase the departure of the dimensionless temperature profile from linearity. When these temperatures are not equal, the two-phase model solution, represented by

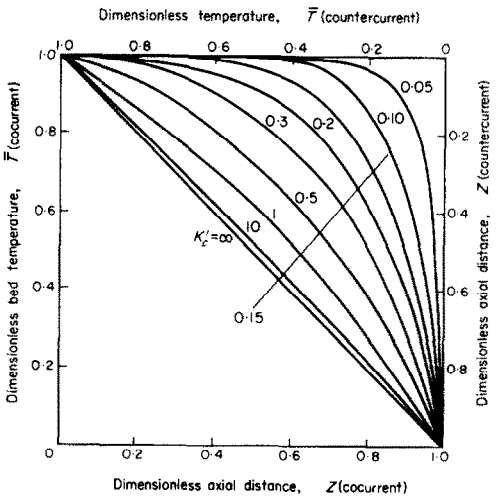

FIG. 3. Continuous model solution for equal gas and solid temperatures for both cocurrent and countercurrent gas and heat flows, parameter $K_C' = K_C + 1/Pe_C$.

equations (7) and (8) of Appendix 1, is as shown in Fig. 4 with the Péclét number, Pe, as a parameter. For $Pe = 0{\cdot}5$–$2{\cdot}0$, there is little change in

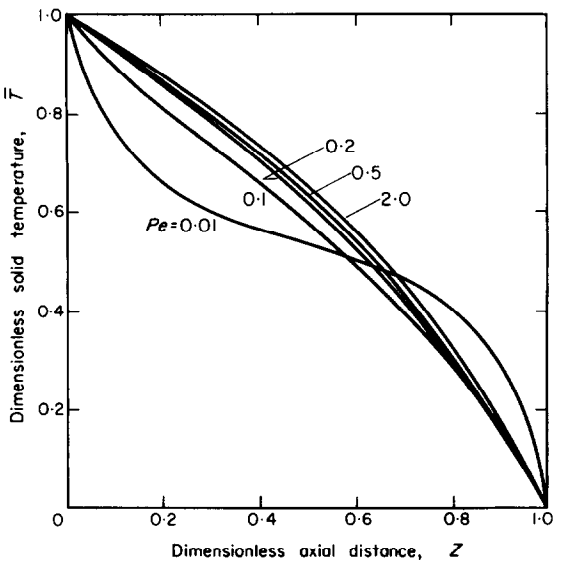

FIG. 4. Exact continuous model solution–effect of Peclet number, for $\bar{t}_o = 1{\cdot}0$, $K_C = 0{\cdot}75$, $H_C = 100$, $Pe_C = 10Pe$.

the profiles, the effect of Pe being less further through the beds. The conduction and convection parameters, K_C and H_C, have a similar influence to that found later in Figs. 6 and 7 with the equivalent mixing cell parameters, K_D and H_D.

The effect of radiant heat transfer within the bed can only be allowed for in this continuous model by including it in the effective solid conductivity if analytical solutions are required.

The discrete deterministic conduction–convection model

This model for gas flow through a packed bed considers the equivalent physical model of gas flow through an array of perfectly mixed tanks or cells. These are arranged in series for one-dimensional models [7–9] or branch radially for higher dimensions [10–12], the number m of sequential cells equivalent to the bed length being chosen to give the correct amount of axial dispersion. An analogy to this is found in the continuous model's choice of a tortuosity factor, ψ, for the gas phase conduction contribution.

Heat transfer processes in the bed are thus considered in a sequence of finite stages, allowing for finite discontinuities in passing from one mixing cell to another. Most discrete packed bed models have only been discussed for isothermal fluid mixing and mass transfer [5] or for the simplest heat transfer situation. Thus, for the latter, specifying a constant solid temperature, T, throughout the bed as in constant rate drying, the solution is [13] $(t_0 - T)/(t_m - T) = (1 + H_D)^m$.

A more general discrete or mixing cell model is developed in Appendix 2 to account for conduction and convection in a packed bed with non-equal gas and solid temperatures. The gas is considered to flow through a sequence of m equal cells, each perfectly mixed and of cross-sectional area ε and length l. This arrangement, indicated in Fig. 5, can account for heat transfer by bulk flow and also for axial mixing or dispersion within the gas (mechanism 10). The solid phase in the bed is represented by a rod stretching the bed length L and of any arbitrary shape, but of cross-section area $(1 - \varepsilon)$, and a surface area Sl, in contact with the fluid in a given cell. Interphase convection heat transfer (mechanism 9) and axial conduction in the solid phase can thus be accounted for. Thermal conductivity in the solid normal to gas flow is considered to be infinite so that the the model represents essentially a one-dimensional process but allows local interphase variations normal to this direction. Property parameters represented by H_D for convection, K_D for conduction, and P_D for the point resistance can be freely varied between stages, but are constant within a given stage.

This model is capable of greater sophistication to account more closely for local void mixing characteristics such as stagnant or bypassing fluid regions, using mixed models consisting of various interconnected arrangements of perfectly mixed regions, stagnant volumes and plug flow regions [14–17], as well as for variations such as local voidage in the bed structure.

The inclusion of radiation as a specific mechanism adds very considerably to the complexity

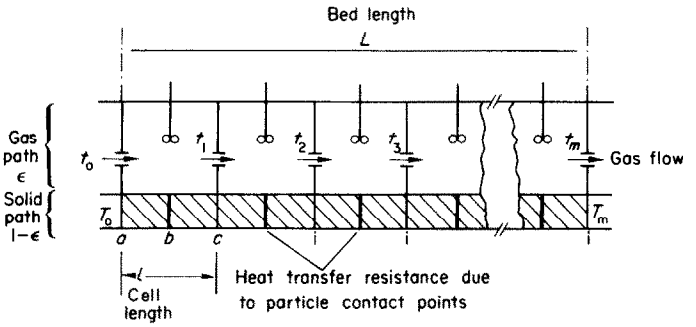

FIG. 5. One-dimensional mixing cell model for conduction and convection in a packed bed with non-equal gas and solid temperatures.

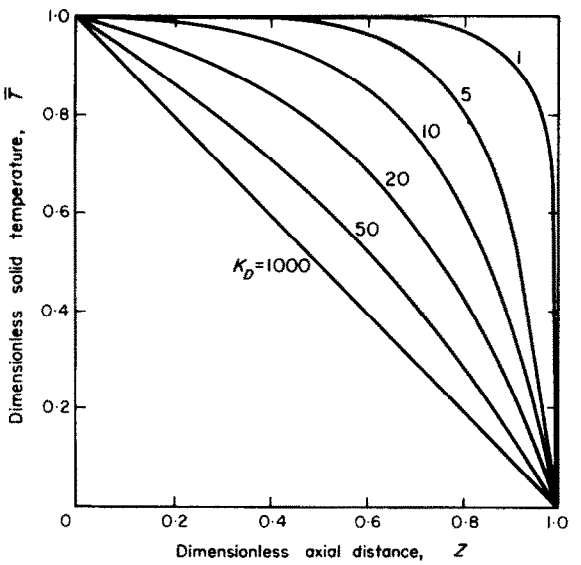

FIG. 6. Effect of the conduction parameter, K_D, on the mixing cell model solid temperature profile for model parameter values: $t_0 = 1{\cdot}0$, $H_D = 10$, $P_D = 0$, $m = 55$.

of the model solution. However, as in the continuous model, a suitable modification of the value of the effective thermal conductivity of the solid can be made to include radiation. Alternatively, radiation effects can be incorporated in the contact point parameter P_D, by equating (2) the conduction resistances from the mixing cell model and from the stagnant gas conduction–radiation model [Part I, equation (7)].

The equations for the discrete model are given in Appendix 2, along with the solution for the case in which the parameters (evaluated as in Appendix 3) are constant throughout the bed length. Further detail is given elsewhere [2]. The inlet gas temperature has little effect on the solid temperature profile but Fig. 6 illustrates the increased curvature obtained for decreased values of the conduction parameter. Similar effects are obtained for decreased values of the contact point parameter or for increased values

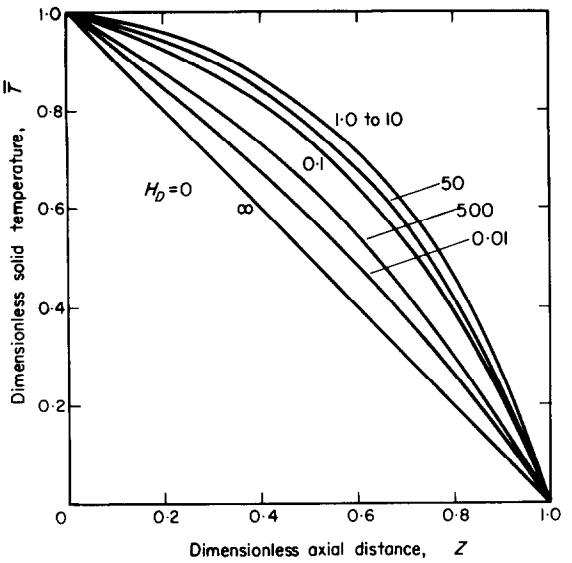

FIG. 7. Effect of the convection parameter, H_D, on the mixing cell model solid temperature profile for model parameter values: $\bar{t}_0 = 1{\cdot}0$, $K_D = 17{\cdot}5$, $P_D = 0$, $m = 55$.

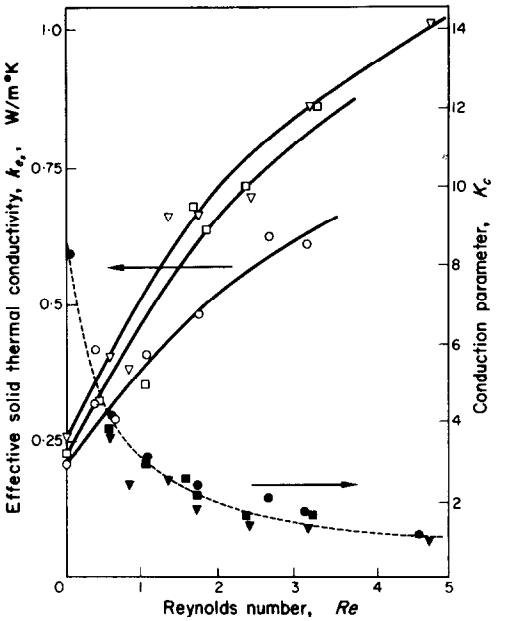

FIG. 8. Continuous model conduction parameter, K_C, and effective thermal conductivity (T_0 values: ○● 180°, □■ 450°C, ▽▼ 650°C).

of the Reynolds number or number of mixing cells. Figure 7 indicates that larger values of the convection parameter initially give very curved profiles which reach a limit with values of H_D between 1 and 10 but then with larger values return to the linear form. Appendix 3 also relates the mixing cell model parameters m, H_D, K_D, P_D to the continuous model parameters Pe_C, H_C and K_C.

4. ANALYSIS

Data evaluation in terms of continuous model

The solution of the continuous model based upon assumed equal solid and gas temperatures was used to derive effective thermal conductivity values from dimensionless experimental temperature profiles such as in Fig. 2. The conductivity value thus derived lumps together the effect of all the conduction and radiation mechanisms along with the gas–solid convection contribution. The bulk flow and convection contribution was included explicitly in the model. The effective thermal conducitivity at a given gas flow rate was determined from the value of the parameter K_C which yielded a continuous model profile (Fig. 3) corresponding most closely to the slope of the experimental dimensionless profile at the bed exit. Figure 8 shows values of K_C and k_{e_s} derived in this way, and the relative effects of gas–solid convection and radiation mechanisms.

Data evaluation in terms of discrete model

The present discrete mixing cell model is dependent on parameters H_D, K_D and P_D. If P_D is set to zero and the effective conduction parameters K_D allowed to include contact resistance as well as any radiation effect (Appendix 3d), a simpler analysis results. This, however, is still able to yield more information concerning the heat transfer mechanisms than the continuous model since the gas–solid convection mechanism is isolated.

The parameter H_D was obtained from a known J_h correlation [18] and K_D then deduced by

regression [2] of the area under the experimental and model profiles.

Figure 9 shows the values of K_D and k_{e_s} as functions of a particle Reynolds number for three hot-face bed temperature levels. It is seen that for $Re < 1$ the values of K_D decrease

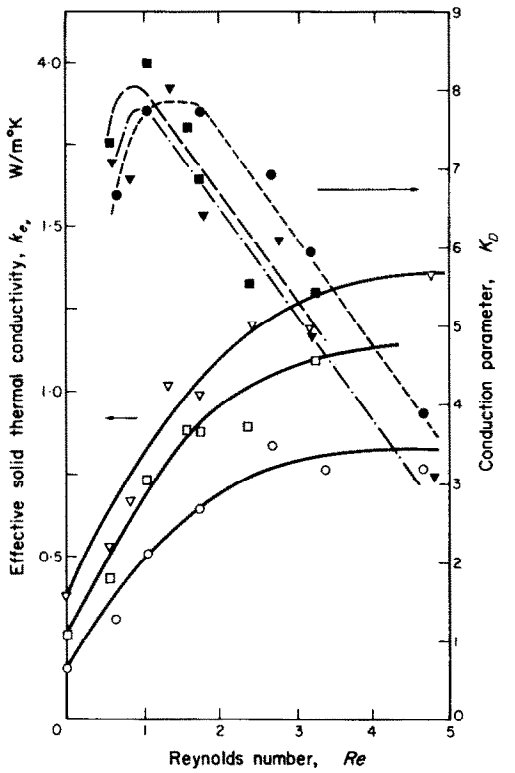

FIG. 9. Mixing model conduction parameter, K_D, and effective solid thermal conductivity for gas flow runs (T_0 values: ○● 180°, □■ 450°, ▽▼ 650°C).

significantly due to the effect of natural convection accentuating the stagnant profile curvature. Figure 9 also shows that k_{e_s} initially increases linearly with the Reynolds number from the stagnant gas values, but tends to constant values by about $Re = 3$. This is due to increasing values of the Péclét number in the range $Re = 0$–3 giving increased void mixing of the stagnant gas. For $Re > 3$ the Péclét number is approximately constant so that the stagnant film or pendular gas ring around each contact point is not decreased further and the effective thermal conductivity of the solid path remains constant. A similar variation is found with $Y = k_{e_s}/k_g$, but this correlation brings the three k_{e_s} curves of Fig. 9 into a single curve reaching a limiting value of about 22 above $Re = 3$. The effect of temperature level is to increase these conductivity values. The gas flow has more effect on the effective conduction in the bed at lower temperatures, as expected. The effect of radiation at the higher bed temperature levels is apparent at all flow rates.

Gas–solid temperature difference from the mixing cell model

Figure 10 shows that the divergence of the gas exit temperature, as calculated from the mixing cell model, from the experimental values of the solid exit temperature ($\bar{T}_m = 0$) increases with increased Reynolds numbers above unity. The dimensionless value of $\bar{t}_m = 0{\cdot}1$ at $Re = 3{\cdot}4$ indicates that it is not generally adequate to assume equal gas and solid temperatures.

Axial heat flow rate from the mixing cell model

The effect of Reynolds number on the mixing cell model heat flow parameter, Q_D, is seen in Fig. 10 for the present experimental results. From this information the axial flow rates, Q, can be calculated from equation (20). Figure 11 shows that these values increase linearly with flow rate, at a greater rate for the higher temperature levels and tend to the stagnant profile heat flow rates as $Re \to 0$.

Temperature profiles using the mixing cell model parameter, P_D

The values of the parameter P_D, evaluated as described earlier, include the effects of contact point resistance and the radiation mechanisms and are shown in Fig. 11 as a function of temperature. The temperature profiles were then given directly by the mixing cell model solution [equations (14) and (15)] using the conduction parameter K_D based on the solid thermal conductivity k_s (Appendix 3d), and the parameters m and H_D from equations (16)

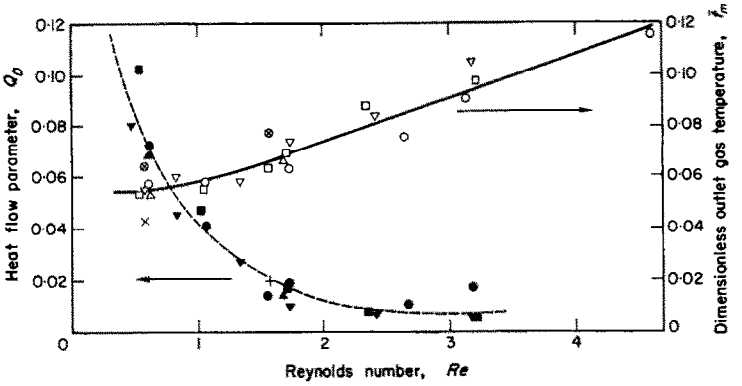

FIG. 10. Outlet gas temperatures (derived from mixing cell model) and mixing cell model heat flow parameter, Q_D, for gas flow runs (T_0 values: ○● 180°, ⊗× 280°, □■ 450°, △▲ 520°, ▽▼ 650°).

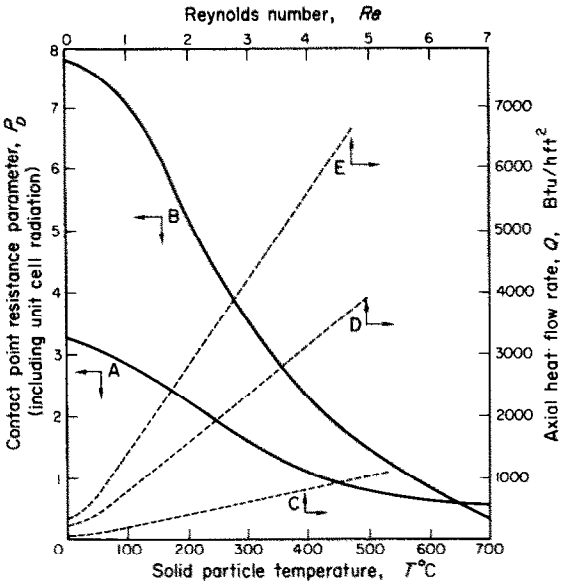

FIG. 11. Mixing cell model contact point resistance parameter, P_D, derived from the stagnant bed effective thermal conductivity (curve A: gas in parallel path is completely mixed, B: all gas in unit cell is completely mixed) and axial heat flow rates for gas flow runs (T_0: C: 180°C, D: 450°C, E: 650°C).

and (17). Good correspondence between the model and the experimental profiles was obtained, particularly when complete mixing of the unit cell gas in the parallel path was assumed in the model.

Relative contributions of the gas flow convection mechanisms

Table 1 shows some typical values of the relative heat flow parameters ϕ_A and ϕ_B, the latter being defined in Appendix 3f. The value of ϕ_A expresses the ratio of the heat flow in the solid to the heat flow in the gas and is thus a measure of the bulk gas flow convection contribution. The value of ϕ_A varies along the length of the bed and the values shown in Table 1 are integrated mean values. It can be seen that increased Reynolds numbers markedly increase the bulk gas flow contribution although increased temperature has little effect. At high temperatures therefore the increased radiation contributions must be counterbalanced by an increased gas enthalpy.

Table 1. Relative heat flow parameters, ϕ_A, ϕ_B

Re	Bed midpoint temperature, °C	(ϕ_A) average	ϕ_B
0·61	159·5	0·65	0·39
3·14	175·0	0·17	0·27
0·59	554·9	0·70	0·39
3·19	647·0	0·13	0·30

The value of ϕ_B relates the enthalpy change of the gas to the total axial heat flow and is thus a measure of the gas–solid convection heat

contribution. The values of ϕ_B in Table 1 indicate that this is a significant mechanism and it is relatively unaffected by increased gas flow or bed temperature.

The relative contributions of the conduction and radiation mechanisms under gas flow conditions may be estimated from Table 1 of Part I together with the value of ϕ_A. The fraction of the total heat flow by the gas is $1/(1 + \phi_A)$ and the fraction of the total heat flow through the the solid is $\phi_A/(1 + \phi_A)$. Thus the contributions shown in that table are diminished by this ratio when gas flows through the bed. Under these conditions there is also no contribution from the gas parallel path although this has little effect. Thus using an average value for ϕ_A of 0·41 this reduces the percentage contribution shown in the Part I table by multiplying them by the fraction 0·29.

Conduction–convection mechanisms based on published experimental results

Effective solid phase thermal conductivity from the diffusion model. There appears to be no gas flow results in the literature at temperatures such that radiation is significant. For countercurrent gas and heat flow at lower temperatures, less than 150°C, Yagi, Kunii and Wakao [21] and Ikeda, Nishimura and Kubota [22] obtained less increase in k_e with increased Reynolds number than shown by the present cocurrent results (Fig. 8). In the latter the gas to solid heat transfer ($t > T$ since $\bar{t}_o \geqslant 1$ in these experiments) increases the solid phase heat flow and hence the effective solid thermal conductivity is greater in contrast to the countercurrent case where the solid to gas heat transfer ($T > t$) gives a lower solid phase heat flow and hence a lower effective solid conductivity.

Effective solid phase thermal conductivity from the mixing cell model. The countercurrent data of Yagi, Kunii and Wakao [21] enabled the mixing cell model to be applied [2] to a greater range of Reynolds numbers (1·03–52·3) than was possible in the present experimental work, as well as to a range of solid thermal conductivities. From Table 2, it is seen that K_D is inversely proportional to Reynolds number indicating that the limiting constant values of the bed thermal conductivity and Y have been reached in this range of Reynolds number. This is also confirmed in Fig. 12. Table 2 shows that conduction with gas flow in the bed as characterised by the ratio Y/Y_{stag} is approximately constant at 1·5–1·8 for all granular packings, with a slightly lower value for Raschig rings. These countercurrent ratios are lower than the cocurrent values of 3·1 for a comparable temperature level in the present experiments. This is due to the respective positive and negative values of $(T - t)$ as noted in the previous section. Figure 12 shows values for one packing of the ratio H_D/K_D which is a measure of the relative importance of solid–gas convection compared with conduction. The increase in H_D/K_D with Reynolds numbers is most pronounced at low values of Reynolds number, as would be expected.

Table 2. Mixing cell model analysis of the data of Yagi, Kunii and Wakao [21]

Packing	D_p, mm	ε	X	Re	$\frac{(\ln K_D)}{(\ln Re)}$ (least squares slope)	$Y_{average}$	$\frac{Y}{Y_{stag}}$
Glass beads	0·91–6·0	0·40	24·0	0·89–12·6	0·990 ± 0·038	13·5	1·8
Limestone broken pieces	1·3 –3·4	0·43	57·6	2·0 –12·9	0·902 ± 0·027	17·6	1·8
Porcelain Raschig Rings	4·0 –9·0	0·50–0·69	67·4	10·9 –27·3	1·19 ± 0·035	8·2	1·2
Steel balls	3·0 –4·8	0·40	1922	14·6 –38·7	1·03 ± 0·039	19·3	1·5

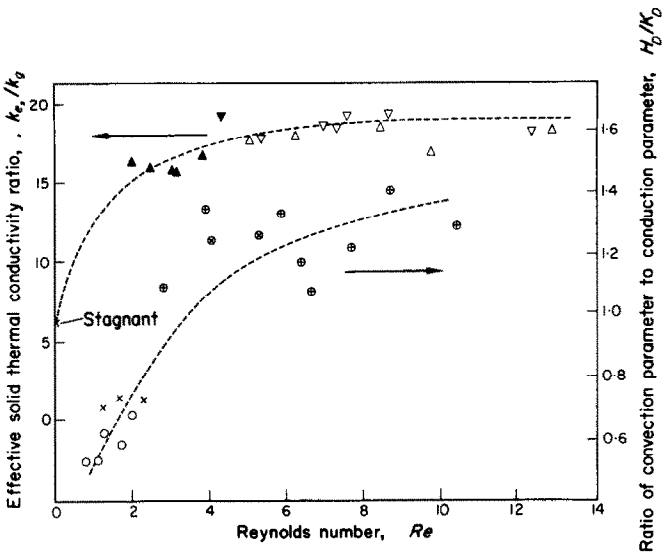

FIG. 12. Mixing cell model effective solid thermal conductivity ratios for limestone: ▲ 1·3 mm, ▽ 2·0 mm, △ 3·4 mm D_p and the ratio H_D/K_D, for glass: ○ 0·91 mm, ⊗ 2·6 mm, ⊕ 6·0 mm. D_p from the data of Yagi, Kunii and Wakao [22].

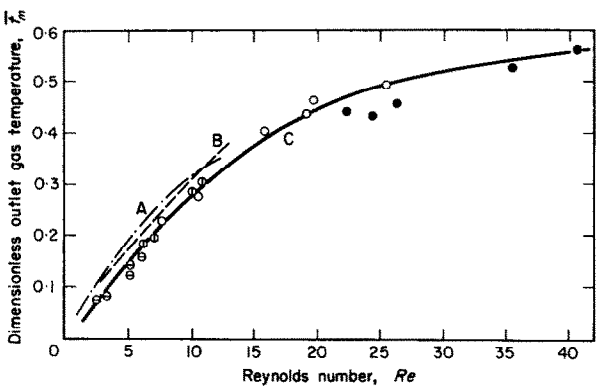

FIG. 13. Mixing cell model dimensionless outlet gas temperatures for the data of Yagi, Kunii and Wakao [22] (Curve A = glass, Curve B = limestone, Curve C = steel and lead; Steel: ● 4·8 mm. D_p, 50 mm. D_T; ○ 4·8 mm. D_p, 68 mm. D_T; ⊙ 3·0 mm. D_p, 68 mm. D_T. Lead: ⊖ 1·5 mm. D_p, 68 mm. D_T).

Solid–gas temperature difference from the mixing cell model. Figure 13 shows how the solid–gas temperature difference at the hot face end of the bed ($Z = 1$ for the countercurrent case) increases markedly with Reynolds number but it is not very dependent on the solid particle thermal conductivity. For $Re < 5$ the values are similar to the present cocurrent results. For $Re > 5$, these values of $\bar{t}_m$ indicated that the assumption of equal solid and gas temperatures used by Yagi *et al.* [21] in applying the continuous model was unjustified.

5. CONCLUSIONS

Conceptually simple models have been developed to evaluate the various mechanisms controlling axial heat transfer in packed beds and compared with experimental data. The common assumption of literature models of equal solid and gas temperatures has been shown to be generally unjustified. For average conditions tested here, about 30 per cent of the axial heat flow occurs through the combined solid paths, the rest being due to bulk gas flow convection. The importance of bulk flow however is a direct function of gas flow but relatively unaffected by temperature levels. For high temperature reacting gas–solid industrial systems, convection, radiation and conduction mechanisms will all contribute, their order of importance decreasing in this sequence.

The continuous or diffusion model indicated that the value of the effective solid thermal conductivity ratio, Y (based on bed area and including interphase terms), increased linearly with Reynolds number from its stagnant bed value, the slope being greater for cocurrent than countercurrent operation, and for low compared to high temperatures. The discrete or mixing model however yielded more information. Values of Y based on solid area were found to initially increase with Reynolds number, but eventually tending to constant values. This latter condition resulted in values of Y/Y_{stag} equal to 3·1 and about 1·6 for cocurrent and countercurrent low low temperature operations respectively.

REFERENCES

1. G. S. G. BEVERIDGE and D. P. HAUGHEY, Axial heat transfer in packed beds, Stagnant beds between 20 and 750°C, *Int. J. Heat Mass Transfer* **14**, 1093–1113 (1971).
2. D. P. HAUGHEY, Axial heat transfer in packed beds, Ph.D. Thesis, Edinburgh University (1966).
3. Y. KATTO and T. MASUOKA, Criterion for the onset of convective flow in a fluid in a porous medium, *Int. J. Heat Mass Transfer* **10**, 297–309 (1967).
4. D. E. LAMB and R. H. WILHELM, Effects of packed bed properties on local concentrations and temperature patterns, *Ind. Engng Chem. Fundls* **2**, 173–182 (1963).
5. D. M. HIMMELBLAU and K. B. BISCHOFF, *Process Analysis and Simulation—Deterministic Systems*. J. Wiley, New York (1968).
6. D. M. HIMMELBLAU, *Process Analysis by Statistical Methods*. J. Wiley, New York (1970).
7. C. B. ROSAS, Axial mixing and selectivity, *Ind. Engng Chem. Fundls* **8**, 361–364 (1969).
8. R. ARIS and N. R. AMUNDSON, Some remarks on longitudinal mixing or diffusion in fixed beds, *A.I.Ch.E.Jl* **3**, 280–282 (1957).
9. J. COSTE, D. RUDD and N. R. AMUNDSON, Taylor diffusion in tubular reactors, *Can. J. Chem. Engng* **39**, 149–151 (1961).
10. H. A. DEANS and L. LAPIDUS, A computational model for predicting and correlating the behaviour of fixed bed reactors; I—Derivation of model for non-reactive systems, *A.I.Ch.E.Jl* **6**, 656–668 (1960).
11. J. E. CRIDER and A. S. FOSS, Effective wall heat transfer coefficients and thermal resistances in mathematical models of packed beds, *A.I.Ch.E.Jl* **11**, 1012–1019 (1965); also Univ. California Radiation Lab. Rept. UCRL-11757 (1965).
12. M. L. MCGUIRE and L. LAPIDUS, On the stability of a detailed packed bed reactor, *A.I.Ch.E.Jl* **11**, 85–95 (1965).
13. N. EPSTEIN, Correction factor for axial flow in packed beds, *Can. J. Chem. Engng* **36**, 210–212 (1958).
14. O. LEVENSPIEL, *Chemical Reaction Engineering*. J. Wiley, New York (1962).
15. O. LEVENSPIEL and K. B. BISCHOFF, Patterns of flow in chemical process vessels, *Adv. Chem. Engng* **4**, 95–198. Academic Press, New York (1963).
16. A. CHOLETTE and L. CLOUTIER, Mixing efficiency determinations for continuous flow systems, *Can. J. Chem. Engng* **37**, 105–112 (1959).
17. A. CHOLETTE and J. BLANCHET, Optimum performance of combined flow reactors under adiabatic conditions, *Can. J. Chem. Engng* **39**, 192–198 (1961).
18. J. E. WILLIAMSON, K. E. BAZAIRE and C. J. GEANKPOLIS, Liquid-phase mass transfer at low Reynolds numbers, *Ind. Eng. Chem. Fundls* **2**, 126–129 (1963).
19. K. B. BISCHOFF and O. LEVENSPIEL, Fluid dispersion—generalization and comparison of mathematical models: I—Generalization of models, *Chem. Engng Sci.* **17**, 245–255 (1962); II—Comparison of models, *ibid.* **17**, 257–263 (1962).
20. R. H. WILHELM, Progress towards the *a priori* design of chemical reactors, *Pure Appl. Chem.* **5**, 403–421 (1962).
21. S. YAGI, D. KUNII and N. WAKAO, Effective thermal conductivities in packed beds, *A.I.Ch.E.Jl* **6**, 543–546 (1960).
22. M. IKEDA, Y. NISHIMURA and H. KUBOTA, On the mechanism of heat transfer in packed bed. *Chem. Engng Japan* **28**, 350 (1964).
23. E. SINGER and R. H. WILHELM, Heat transfer in packed beds, analytical solution and design method, fluid flow, solids flow and chemical reaction, *Chem. Engng Prog.* **46** (7), 343–357 (1950).
24. G. S. G. BEVERIDGE, A survey of interphase reaction and exchange in fixed and moving beds, Dept. Chem. Eng., University of Minnesota (1962).
25. J. F. WEHNER and R. H. WILHELM, Boundary conditions of flow reactor, *Chem. Engng Sci.* **6**, 89–93 (1956).
26. P. V. DANCKWERTS, Continuous flow systems—distri-

bution of residence times, *Chem. Engng Sci.* **2**, 1–13 (1953).
27. H. KRAMERS and G. ALBERDA, Frequency response analysis of continuous flow systems, *Chem. Engng Sci.* **2**, 173–181 (1953).
28. L. T. FAN and R. BAILIE, Axial diffusion in isothermal tubular flow reactors, *Chem. Engng Sci.* **13**, 63–68 (1960).
29. O. LEVENSPIEL and K. B. BISCHOFF, Backmixing in the design of chemical reactors, *Ind. Engng Chem.* **51**, 1431–1439 (1959).
30. J. R. A. PEARSON, A note on the "Danckwerts" boundary conditions for continuous flow reactors, *Chem. Engng Sci.* **10**, 281–284 (1959).
31. L. T. FAN and Y. K. AHN, Critical evaluation of boundary conditions for turbulent flow reactors, *Ind. Engng Chem. Proc. Des. & Dev.* **1**, 190–195 (1962).
32. K. B. BISCHOFF, A note on boundary conditions for flow reactors, *Chem. Engng Sci.* **16**, 131–133 (1961).
33. P. ADIVARAHAN, D. KUNII and J. M. SMITH, Heat transfer in porous rocks through which single-phase fluids are flowing, *Soc. Petrol. Engrs Jl* **2**, 290–296 (1962).
34. H. S. CARSLAW and J. C. JAEGAR, *Conduction of Heat in Solids*. Oxford Univ. Press (1948).

APPENDICES—MATHEMATICAL MODELS FOR CONDUCTION AND CONVECTION PROCESSES IN A PACKED BED

Appendix 1: *One-dimensional Continuous Model* [2]

For steady state heat transfer in a packed bed composed of separate gas and solid continuous homogeneous phases, the general differential energy balances [23, 24] applied to the present experimental system with only a spatial variation in the axial direction, z, parallel to the gas flow, reduce to the following dimensionless forms for the two-phase system

$$\frac{1}{Pe_C}\frac{\partial^2 \bar{t}}{\partial Z^2} - \frac{\partial \bar{t}}{\partial Z} + H_C(\bar{T} - \bar{t}) = 0 \tag{1}$$

$$K_C\frac{\partial^2 \bar{T}}{\partial Z^2} - H_C(\bar{T} - \bar{t}) = 0 \tag{2}$$

and for the single pseudo-homogeneous phase

$$K'_C\frac{\partial^2 \bar{T}}{\partial Z^2} - \frac{\partial \bar{T}}{\partial Z} = 0 \tag{3}$$

where $Z = z/L$; $\bar{t} = (t - T_m)/(T_0 - T_m)$; $\bar{T} = (T - T_m)/(T_0 - T_m)$; $Pe_C = GL/\rho E$;

$$K_C = k_{es}(1 - \varepsilon)/GC_gL; \quad H_C = hSL/GC_g;$$

$$\text{and} \quad K'_C = K_C + 1/Pe_C.$$

It can then be found [8] that the boundary conditions on the bed

$$\bar{t}_* = \bar{t}_0 - \frac{1}{Pe_C}\left(\frac{\partial \bar{t}}{\partial Z}\right)_0 \tag{4}$$

and

$$\left(\frac{\partial \bar{t}}{\partial Z}\right)_1 = 0 \tag{5}$$

will apply at the bed entry and exist respectively. Called the Danckwerts boundary conditions they have found frequent application [25–31], being correct under all steady state conditions [32]. For the solid phase, the solid temperatures at the bed entry and exit are specified, so that

$$\bar{T} = 1 \text{ at } Z = 0 \text{ and } \bar{T} = 0 \text{ at } Z = 1. \tag{6}$$

For the single phase system, with equal gas and solid temperatures, the only boundary conditions on equation (3) will be those of equation (6).

The general solutions for both the single and two-phase approaches can be derived from the following general solution (particular solutions being also published [22, 24, 33]) for various conditions including infinite and finite Peclet numbers and finite and infinite bed lengths. The general solution for the two-phase system represented by equations (1) and (2) is

$$\bar{T} = C_4 + \sum_{i=1}^{3} C_i e^{F_i Z} \tag{7}$$

$$\bar{t} = C_4 + \sum_{i=1}^{3} C_i e^{F_i Z}(F_i^2 - K_C/H_C) \tag{8}$$

where F_i are the roots of

$$F^3 - Pe_C F^2 - F(1 + K_C Pe_C)H_C/K_C + Pe_C H_C/K_C = 0$$

and the constants C_i are given by

$$\begin{bmatrix} F_1\left(F_1^2 - \frac{K_C}{H_C}\right)e^{F_1} & F_2\left(F_2^2 - \frac{K_C}{H_C}\right)e^{F_2} & F_3\left(F_3^2 - \frac{K_C}{H_C}\right)e^{F} & 0 \\ e^{F_1} & e^{F_2} & e^{F_3} & 1 \\ F_1 & F_2 & F_3 & 1/K_C \\ 1 & 1 & 1 & 1 \end{bmatrix}\begin{bmatrix} C_1 \\ C_2 \\ C_3 \\ C_4 \end{bmatrix} = \begin{bmatrix} 0 \\ 0 \\ -\bar{t}_*/K_C \\ 0 \end{bmatrix}$$

Appendix 2: *One-dimensional Mixing Cell Model* [2].

For the model generally described in Section 3 and by Fig. 5, the temperature at any distance z along a solid rod

in which heat transfer takes place both by axial conduction and by surface transfer to a gas of uniform temperature, t_{r+1}, is given [34] by

$$T_z - t_{r+1} = C_5 e^{CZ'} + C_6 e^{-CZ'} \tag{9}$$

where $C = \sqrt{(H_D/K_D)}$, $H_D = hSl/GC_g$, $K_D = k_s(1-\varepsilon)/GC_g l$ (Appendix 3d) and $Z' = z/l$. Boundary conditions on the solid at its mid-point in the cell, $z = b$, are found from a heat balance

$$-k_s(1-\varepsilon)\left(\frac{\partial T}{\partial z}\right)_{b-} = h_p(1-\varepsilon)(T_{b-} - T_{b+})$$

$$= -k_s(1-\varepsilon)\left(\frac{\partial T}{\partial z}\right)_{b+}$$

so that

$$T_{b-} - T_{b+} = -P_D\left(\frac{\partial T}{\partial Z'}\right)_{b+} \tag{10}$$

and

$$\left(\frac{\partial T}{\partial Z'}\right)_{b-} = \left(\frac{\partial T}{\partial Z'}\right)_{b+} \tag{11}$$

where $P_D = k_s/lh_p$. Equations (9)–(11) allow the solid temperature profile to be derived as a function of the cell gas temperature t_{r+1}, and the solid temperature and gradient at the cell inlet, $T_a = T_r$, and $(\partial T/\partial Z')_a \equiv (\partial T/\partial Z')_r$. In particular this gives the solid temperature $T_c \equiv T_{r+1}$, at the cell exit ($z = c$), as

$$T_c - t_{r+1} = \left(\frac{\partial T}{\partial Z'}\right)_a\left[\frac{\sinh C}{C} + \frac{P_D}{2}(\cosh C + 1)\right] + (T_a - t_{r+1})\left[\cosh C + \frac{P_D}{2}\sinh C\right] \tag{12}$$

while a heat balance over the cell gives

$$Q = GC_g t_r - k_s(1-\varepsilon)\left(\frac{\partial T}{\partial z}\right)_r = GC_g t_{r+1} - k_s(1-\varepsilon)\left(\frac{\partial T}{\partial z}\right)_{r+1}$$

where Q is the heat flux, so that $Q'_D = Q/GC_g$ is given by

$$Q'_D = t_r - K_D\left(\frac{\partial T}{\partial Z'}\right)_r = t_{r+1} - K_D\left(\frac{\partial T}{\partial Z'}\right)_{r+1} \tag{13}$$

Thus starting from the cell inlet conditions, t_r, T_r and $(\partial T(\partial Z'))_r$ equations (12) and (13) enable corresponding values to be determined at the cell outlet as a function of the parameters, H_D, K_D and P_D. A stepwise solution can thus be carried out from the bed inlet for m successive stages. Values for any point within a cell can be determined from equation (9).

If the model parameters are constant throughout, an analytical solution may be obtained [2] as

$$\bar{t}_r = \frac{[2B^r(BD-1) - B^m(B+1)(D-1)] + W_1[2D^r(BD-1) - D^m(B-1)(D+1)]}{W_2} \tag{14}$$

$$T_r = \frac{[(B+1)(D-1)(B^r - D^m)] + W_1(B-1)(D+1)(D^r - D^m)}{W_2} \tag{15}$$

where

$$W_1 = -\frac{(B+1)(D-1)[B^m - \bar{t}_\delta(1-B^m)] - 2B^\delta(BD-1)}{(B-1)(D+1)[D^m - \bar{t}_\delta(1-D^m)] - 2D^\delta(BD-1)}$$

with $\delta = 0$ or m, and

$$W_2 = (B+1)(D-1)(1-B^m) + W_1(B-1)(D+1)(1-D^m)$$

$$B = -W_3[1 + (1 - 4W_4/W_3^2)^{\frac{1}{2}}]/W_4$$

$$D = -W_3[1 - (1 - 4W_4/W_3^2)^{\frac{1}{2}}]/W_4$$

$$W_3 = 1 + \sqrt{(H_D K_D)}\sinh\sqrt{\left(\frac{H_D}{K_D}\right)} + \frac{H_D P_D}{2} \times \left(\cosh\sqrt{\left(\frac{H_D}{K_D}\right)} - 1\right)$$

$$W_4 = \frac{H_D P_D}{2} - \left[\sqrt{(H_D K_D)} + P_D\sqrt{\left(\frac{H_D}{K_D}\right)}\right] \times \sinh\sqrt{\left(\frac{H_D}{K_D}\right)} - \left(2 + \frac{H_D P_D}{2}\right)\cosh\sqrt{\left(\frac{H_D}{K_D}\right)}$$

Equations (14) and (15) allow the determination of the solid temperatures at the end of each cell and the gas temperature within the cell as a function only of H_D, K_D, P_D, m and $\bar{t}_0$ or $\bar{t}_m$. These parameters are discussed in Appendix 3 Intermediate solid temperature values can be found by the use of equation (9).

Appendix 3: Evaluation of the Mixing Cell Model Parameters [2]

(a) *Number of mixing cells*, m

The limiting value for relatively long beds at high Reynolds number is given by

$$m = \frac{Pe_C}{2} = \frac{Pe}{2}\left(\frac{L}{D_p}\right). \tag{16}$$

A correction for low Reynolds number is required [2, 19, 20].

(b) *Convection parameter*, H_D

This represents the ratio of gas–solid convective heat transfer (mechanism 9) to that by bulk gas flow (mechanism 10) as a convective Stanton number

$$H_D = \frac{hSl}{GCg} = \frac{NuSl}{RePr} = \frac{J_h Sl}{Pr^{\frac{2}{3}}} = \frac{H_c}{m}. \quad (17)$$

(c) *Conduction parameter*, K_D

This is essentially a conduction Stanton number relating heat transfer by effective solid conduction (mechanism 1, 3, 4) to heat transfer by bulk gas flow (mechanism 10), so that

$$K_D = \frac{k_{e_s}(1-\varepsilon)}{GC_g l} = \frac{k_{e_s}}{k_g}\frac{(1-\varepsilon)}{RePr}\frac{D_p}{l} = mK_C. \quad (18)$$

Assuming that K_D is used to represent all the solid paths including point contact, the k_{e_s} value can be derived from the Y ratio (k_e/k_g) deduced for the stagnant bed conduction model, upon omitting the bulk gas contribution.

(d) *Contact point parameter*, P_D

This relates the heat transfer resistance at the point to point contact (mechanisms 3 and 4) to the solid conduction resistance (mechanism 1) as an inverse Nusselt number, so that $P_D = k_s/(h_p l)$. The relationship between K_D (when restricted to the representation of the conduction path only, by $K_D = k_s(1-\varepsilon)/GC_g l$) and P_D for the discrete model and K_C for the continuous model is

$$K_C = K_D/m(1 + P_D). \quad (19)$$

K_D may here include radiation effects but will not account for any contact resistance. If P_D is not used in the discrete model, then the K_D definition of section (c) will apply.

(e) *Heat flux parameter*, Q_D

This can be determined from the basic model parameters by substituting for T from equations (13)–(15) to give the dimensionless form

$$Q_D = \frac{Q'_D - T_0}{T_0 - T_m} \quad (20)$$

$$= [(B+1)(D-1) + W_1(B-1)(D+1)]/W_2 \quad (21)$$

where $Q'_D = Q/GC_g$.

(f) *Relative heat flow parameters* ϕ_A, ϕ_B

Using equation (13) written in dimensionless form, the ratio of the axial heat flow through the solid phase (mechanisms 1, 3, 4) to the heat flow in the gas (mechanism 10) at any distance along the bed length can be written as

$$\phi_A = \frac{-K_D(\partial T/\partial Z')_r}{\bar{t}_r} = \frac{1+Q_D}{\bar{t}_r} - 1. \quad (22)$$

In addition, the enthalpy change in the gas, during flow through the bed, relative to the total axial heat flow rate, Q, is a measure of the importance of the gas–solid convection mechanism (mechanism 9), and is given by

$$\phi_B = \frac{GC_g(t_0 - t_m)}{Q}$$

$$= \frac{\bar{t}_0 - \bar{t}_m}{Q_D + 1/(1 - T_m/T_0)}$$

on using equation (20).

TRANSFERT THERMIQUE AXIAL DANS DES GARNISSAGES. ECOULEMENT GAZEUX DANS DES LITS ENTRE 20 ET 650°C

Résumé—On a étendu les mesures expérimentales et les modèles théoriques décrits dans la première partie au cas de l'écoulement gazeux dans un lit. Des mesures de profil de température sont données pour des gaz à co-courant et des écoulements thermiques axiaux à travers le lit dans un domaine de température compris entre 20 et 650°C et un nombre de Reynolds de particule jusqu'à 5.

Ces résultats sont analysés en fonction d'un modèle continu (de diffusion) et d'un nouveau modèle discret (cellule de mélange). Ce dernier fournit une information plus quantitative sur les mécanismes de transfert thermique considérés car contrairement au premier, l'on tient compte de la conduction et du rayonnement du solide, de la résistance de contact du solide aussi bien que de la convection solide-gaz et du transport de l'écoulement gazeux. On vérifie que le modèle discret convient et par comparaison avec les résultats expérimentaux présents de co-courants à basses et hautes témperatures, et avec des mesures préalablement publiées sur des contre-courants à basse température en utilisant une gamme de matériaux de garnissage.

AXIALE WÄRMEÜBERTRAGUNG IN SCHÜTTUNGEN I. GASSTRÖMUNG DURCH SCHÜTTUNGEN IM BEREICH VON 20 BIS 650°C

Zusammenfassung—Die in Teil I beschriebenen experimentellen Untersuchungen und die theoretischen Modelle erstrecken sich auf den Fall einer Gasströmung durch Schüttungen. Die Temperaturprofile

wurden gemessen bei Parallelströmung des Gases und axialem Wärmestrom in der Schüttung über einen Temperaturbereich von 20 bis 650°C und einer örtlichen Reynolds-Zahl bis 5.

Die Ergebnisse werden vom Standpunkt eines kontinuierlichen Diffusions- und eines neuen diskontinuierlichen Mischzellen-Modells erläutert. Das letztere liefert mehr quantitative Informationen über den nicht einfachen Wärmeübergangs-Mechanismus, da Leitung/Strahlung, Kontaktwiderstand, Festkörper-Gas-Konvektion und Gasströmung besonders berücksichtigt wurden. Die Brauchbarkeit des Mischzellen-Modells wurde durch Vergleich der vorliegenden experimentellen Ergebnisse bei Parallelströmung und bei niederen bzw. hohen Temperaturen mit bereits früher veröffentlichten Ergebnissen bei Gegenströmung mit geringen Temperaturen an einer Reihe von Schüttungsmaterialien gezeigt.

ОСЕВОЙ ТЕПЛООБМЕН В ПЛОТНЫХ СЛОЯХ. II. ФИЛЬТРАЦИЯ ГАЗА ЧЕРЕЗ СЛОЙ В ДИАПАЗОНЕ ТЕМПЕРАТУР ОТ 20° ДО 650°С.

Аннотация—Описанные в части I экспериментальные данные и теоретические модели обобщаются на случай фильтрации газа через слой. Приводятся температурные профили для спутного газавого и осевого теплового потоков через слой в диапазоне изменения температур от 20 до 650°С и числа Рейнольдса для частиц до 5.

Результаты анализируются как с помощью сплошной (диффузионной) модели, так и с помощью новой дискретной модели. Последняя обеспечивает больше количественных данных о механизме теплообмена, поскольку, в отличие от ранее предложенной модели учитываются в отдельности излучение и теплопроводность твердых тел, контактное сопротивление твердых тел, а также конвекция твердых тел и газа и конвекция в основном потоке газа. Пригодность дискретной модели обосновывается сравнением настоящих экспериментальных данных для спутного потока при низких и высоких температурах с ренее опубликованными данными для противоточного потока при низкой температуре, используя диапазон изменения материалов насадки.